Journal of Catalysis 376 (2019) 161–167

Contents lists available at ScienceDirect

Journal of Catalysis

journal homepage: www.elsevier.com/locate/jcat

Ternary supramolecular system for photocatalytic oxidation with air by consecutive photo-induced electron transfer processes

Jiachen He [1], Qiuxia Han *,[1], Jie Li, Zhuolin Shi, Xiaoyun Shi, Jingyang Niu *

Henan Key Laboratory of Polyoxometalate Chemistry, Institute of Molecular and Crystal Engineering, College of Chemistry and Chemical Engineering, Henan University, Kaifeng, 475004 Henan, PR China

ARTICLE INFO

Article history:
Received 18 March 2019
Revised 19 May 2019
Accepted 25 June 2019

Keywords:
Polyoxometalate
Metal-organic framework
Photocatalysis
Ammoxidation
Epoxidation

ABSTRACT

Developing new photocatalysts for settling the tightest bottlenecks that lower efficiency, inferior selectivity and harsh conditions in organic oxidation reactions with air is very significant. Herein, ZnW–DPNDI–**PYI** was achieved by assembling a functional photosensitizer, an oxidation catalyst $[BW_{12}O_{40}]^{5-}$, and an organocatalyst into one single framework. The anion···π and N—H···O hydrogen bonds interactions facilitate the consecutive photo-induced electron transfer (conPET) process for the photocatalytic oxidation by stabilizing the radical-anion intermediate and catalyst-substrate interacted moiety. Besides, N,N′-bis(4-pyridylmethyl)naphthalene diimide (DPNDI) can be excited by visible light, the photogenerated electron and hole would further activate oxygen and substrates, respectively, to give the corresponding redox products. High conversion and selectivity of ZnW–DPNDI–**PYI** in photocatalytic coupling of primary amines and olefins epoxidation with air under visible-light have been demonstrated.

1. Introduction

With increasing concern about green and atom economy of organic oxidation in the synthesis of fine chemicals, employing sustainable and clean O_2 oxidant alternative to oxidants such as PhIO, NaClO, H_2O_2 and *t*-BuOOH has become one of the most significant challenges for chemists [1–4]. However, the tightest bottlenecks that lower efficiency, inferior selectivity, difficulty separation of products and harsh conditions in the photocatalytic oxidation with O_2 have limited the practical application in the industry production [5–7]. Due to the high activity of singlet oxygen ($^1O_2$) and superoxide radicals ($O_2^{\cdot-}$), developing new photocatalysts for achieving the synergy among them is necessary for oxidation with excellent activity and selectivity in a mild condition [8–10]. Many efforts by researchers using different photocatalysts have been devoted in recent years, however, the efficiency still needs to be improved because of limited catalytic centers, weak force from center to center and less energy of a single absorbed photon. [11,12]

Consecutive photo-induced electron transfer process is extremely popular with chemists because it can overcome the current energetic limitation of visible–light photoredox catalysis by using the energies of two photons in one catalytic cycle [13]. Burkhard König et al. reported that subsequent excitation of the perylene diimide (PDI) radical anion accumulates enough energy for the reduction of stable aryl chlorides giving aryl radicals [14]. Duan et al. demonstrated the conPET concept can be extended to a heterogeneous system [15]. However, due to the difficulty on the stabilization of the radical anion formed after the first PET process, the work about conPET process is still limited [16].

In this case, the combination of a photosensitizer and a co-catalyst within a single framework is a powerful approach to generate photocatalysts for prospective practical applications [17–19]. DPNDI is one of the best candidates to satisfy the evaluation of design principles because of its efficient electron-transfer property, high redox activity and strong π-acidity [20]. After visible light irradiation, DPNDI can be excited and the photogenerated hole has strong oxidization. In addition, with the presence of electron donor, DPNDI can form a colored radical anion $DPNDI^{\cdot-}$ that can further be excited by visible light [21]. Polyoxometalates (POMs) are well-known catalysts studied in olefin epoxidation for their stability against oxidative degradation [22,23]. Especially for multielectron transfer process, POMs are the promising applicants because they can accept many electrons and protons without deforming their structures and can produce $O_2^{\cdot-}$ by reduced intermediates [24]. Pyrrolidine-2-yl-imidazole (**PYI**) can act as a suitable electron donor to improve photoinduced electron transfer [25,26].

* Corresponding authors.
E-mail addresses: hdhqx@henu.edu.cn (Q.X. Han), jyniu@henu.edu.cn (J.Y. Niu).
[1] The authors J.C. He and Q.X. Han contributed equally.

https://doi.org/10.1016/j.jcat.2019.06.040
0021-9517/

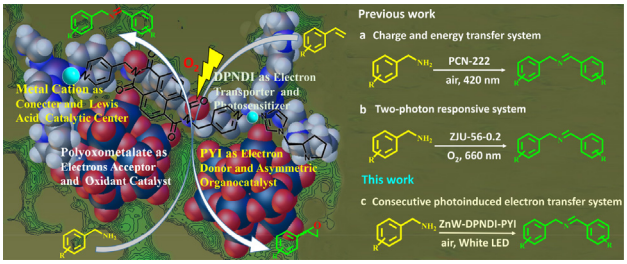

Scheme 1. The design concept for obtaining photocatalysts and representation of selective benzylamine and olefins oxidation over ZnW–DPNDI–**PYI** by photocatalysis.

Herein, a new POM-incorporated metal-organic framework (POMOF) $\{[Zn(HPYI)_3]_2(DPNDI)\}[BW_{12}O_{40}]_2$ (ZnW–DPNDI–**PYI** or **Cat-1,** for short) was synthesized by assembling the $[BW_{12}O_{40}]^{5-}$ anion, zinc (II) ion, DPNDI and PYI within a single framework (Scheme 1). It is ideally suited for heterogeneous photocatalytic conversions owing to the electron donor and acceptor orderly embedded within a photoactive framework. The directional anion···π and C—H···anion interactions between trapped POM anions and π–acidic DPNDI skeletons can promote charge transfer among components, which should contribute to the activation of O_2 [27]. Through conPET process, DPNDI will first form radical anion $DPNDI^{\cdot -*}$, then the $DPNDI^{\cdot -*}$ acts as an electron transporter to transfer electrons to the POM anion [28]. POM anion will act as the electron receiver, which determines the generation of $O_2^{\cdot -}$. PYI moiety in the POMOF will promote the generation of the $DPNDI^{\cdot -}$ as electron donor. In addition, the energy transfer (ET) gives rise to $^1O_2$ generation over naphthalene units by light irradiation [29]. The synergy of $^1O_2$ and $O_2^{\cdot -}$ is beneficial to the excellent catalytic activity and selectivity under ambient conditions.

2. Experimental

2.1. 2.1 preparation

All reagents were used as purchased without further purification. *L*–N-*tert*-butoxy-carbonyl-2-(imidazole)-1-pyrrolidine (***L*–BCIP**) [30], **DPNDI** [31] and $K_5[BW_{12}O_{40}]\cdot 5H_2O$ [32] were prepared according to literature methods and characterized by IR and ^1H NMR. Mixture of $Zn(NO_3)_2\cdot 6H_2O$ (44.6 mg, 0.15 mmol), $K_5[BW_{12}O_{40}]\cdot 5H_2O$ (157.8 mg, 0.05 mmol), DPNDI (23.4 mg, 0.15 mmol) and *L*–BCIP (24.5 mg, 0.1 mmol) for ZnW–DPNDI–**PYI** in mixed water (4.0 mL) and methanol (2.0 mL) was stirred. The resulting suspension was sealed in a 25 mL Teflon-lined reactor and kept at 120 for four days. After cooling the autoclave to room temperature, aqua rod-like single crystals were separated, washed with water and air-dried. (Yield: ca. 60% based on $K_5[BW_{12}O_{40}]\cdot 5H_2O$). Elemental analyses (EA) and ICP calcd (%) for $C_{40}H_{54}N_{14}O_{41}W_{12}Zn_3$: C 12.68, H 1.44, N 5.18, Zn 5.18, W 58.22; Found: C 12.64, H 1.41, N 5.20, Zn 5.22, W 58.24 for ZnW–DPNDI–**PYI**.

2.2. Characterizations

EA of C, H and N were performed on a Vario EL III elemental analyzer. ICP analyses were performed on a Jarrel-AshJ-A1100 spectrometer. FT-IR spectra were recorded as KBr pelletson JASCO FT/IR-430. Powder XRD diffractograms were obtained on a Riguku D/Max-2400. Circular dichroism (CD) spectrum was measured on JASCO J-810. UV–Vis spectra were recorded on a HP 8453 spectrometer. Fluorescent spectra were measured on EDINBURGH F900. The X-ray photoelectron spectroscopy (XPS) measurements were conducted using an ESCALAB 250Xi high-performance electron spectrometer, using monochromatized Al Kα ($h\nu$ = 1486.7 eV) as the excitation source. Mott–Schottky measurements were tested on a CHI 760E electrochemical workstation (Shanghai Chenhua Instrument Co., China) in a three-electrode electrochemical cell using a 0.1 M Na_2SO_4, temperature. ^1H NMR spectra were recorded on a Varian INOVA-400 MHz type (^1H, 400 MHz) spectrometer. The chemical shifts are reported in ppm relative to $CHCl_3$ (δ = 7.26) for ^1H NMR. Optical rotation was measured on a PerkinElmer 241 polarimeter. The photocatalytic reaction were performed on WATTCAS Parallel Light Reactor (WP-TEC-1020HSL) with 10 W COB LED.

2.3. X-ray crystallographic analysis

Crystal with dimensions 0.20 × 0.13 × 0.05 mm for ZnW–DPNDI–**PYI** was stuck on a glass fiber, and intensity data were collected at 296(2) K on a Bruker Smart APEX II CCD diffractometer with graphite-monochromated Mo Kα radiation (λ = 0.71073 Å). Routine Lorentz polarization and Multi-scan absorption correction was applied to intensity data. Its structure was determined and the heavy atoms were found by direct methods using the SHELXTL-97 program package [33]. The remaining atoms were found from successive full-matrix least-squares refinements on F^2 and Fourier syntheses [34,35]. Positions of the hydrogen atoms attached to carbon and nitrogen atoms were geometrically placed. All hydrogen atoms were refined isotropically as a riding mode using the default SHELXTL parameters. Crystallographic data for ZnW–DPNDI–**PYI** were summarized in Table S1.

2.4. Photocatalysis

2.4.1. Typical procedure for the photocatalytic oxidation of amines

A glass tube was filled with amines (5 mmol), ZnW–DPNDI–**PYI** (14 μmol, 0.03 mol%) and acetonitrile (3 mL). The mixture was exposed to a 10 W white LED lamp placed at a distance of 5 cm under air at room temperature. After reaction for 16 h, the mixture was centrifuged to remove ZnW–DPNDI–**PYI** and dried in vacuo. The yield was calculated by integration of the characteristic ^1H NMR peaks of substrates and products.

2.4.2. Typical procedure for the photocatalytic oxidation of olefins

A glass tube was filled with styrene (5 mmol), ZnW–DPNDI–**PYI** (14 μmol, 0.03 mol%) and CH_3CN (3 mL). The mixture was exposed to a 10 W white LED lamp placed at a distance of 5 cm under air at room temperature. After reaction for 12 h, the mixture was centrifuged to remove ZnW–DPNDI–**PYI** and dried in vacuo. The yield was calculated by integration of the characteristic ^1H NMR peaks of substrates and products.

3. Results and discussion

Solvothermal reaction of $Na_5[BW_{12}O_{40}]$, $Zn(NO_3)_2$, *L*–BCIP and DPNDI gave ZnW–DPNDI–**PYI** in a yield of 60%. Elemental analyses and powder X-ray analysis (XRD) indicated the pure phase of its bulk sample (Fig. S1). Single-crystal structural analysis revealed that ZnW–DPNDI–**PYI** crystallizes in the chiral space group $P2_1$ (Table S1). The asymmetric unit of ZnW–DPNDI–**PYI** consists of one cation $\{[Zn(HPYI)_3]_2\ (DPNDI)\}^{10+}$ and two $[BW_{12}O_{40}]^{5-}$ anions (Fig. 1a). Each zinc ion adopts a tetrahedron geometry with four nitrogen atoms from three protonated PYI and one DPNDI (Fig. S2). The Keggin polyanions typically reside directly over the electron-deficient naphthalene ring centroid with centroid distance 3.0 Å (Fig. S3). PYI is in-situ generated with the butoxycarbonyl of BCIP removed in the reaction and the pyrrolidine nitrogen was protonated [36]. The intramolecular strong hydrogen

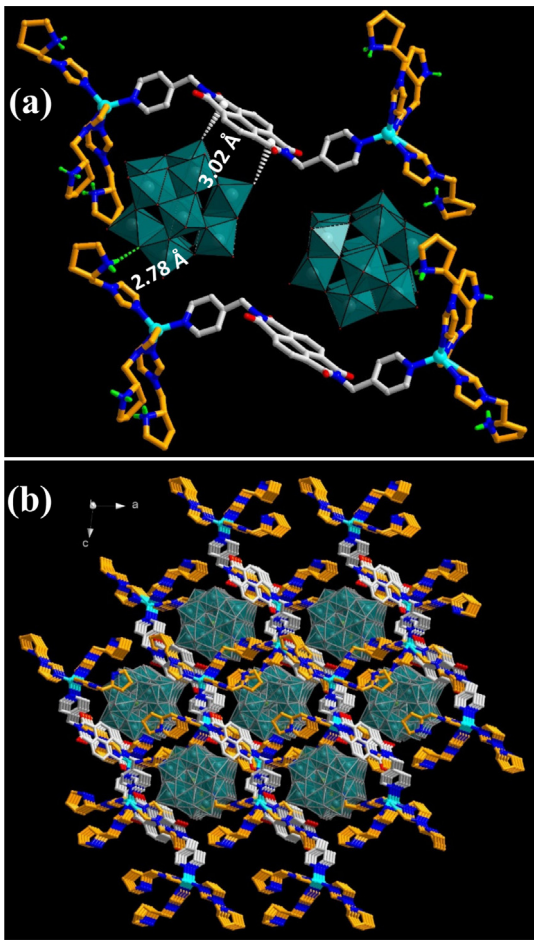

Fig. 1. (**a**) The schematic diagram of the catalytic site distribution in **Cat-1**, showing the interactions of the catalytic sites. (**b**) 3D open network of **Cat-1** viewed down the *b*-axis. H-atoms are omitted for clarity.

bonds formed between hydrogen atoms of DPNDI/PYI molecules and oxygen atoms from the POM can immobilize the functionalized POM and enhance the stability of the structure. These ribbon segments are further stacked to furnish a 3D supramolecular structure by $[BW_{12}O_{40}]^{5-}$, DPNDI and PYI through C—H···O and N—H···O hydrogen bonding interactions (Fig. 1b, Supplementary Table 3). The total solvent-accessible volume accounts for approximately 10.3% of the whole crystal volume as estimated by PLATON [37]. It's postulated that PYI would act as an electron donor to ensure a conPET process, thus improving the catalytic efficiency. Anion···π interactions combined with N—H···O hydrogen bonds not only play important roles in directing the formation of the POMOF but also increase the interactions among the components, which improve the charge transfer and electron exchange, ensuring longer excited-state lifetimes for achieving high activity and selectivity under ambient conditions (Figs. S4–S6). [38,39]

To assess its ability to activate O_2, **Cat-1** was examined in the photocatalytic oxidative homocoupling of amines into imines with air as an oxidant in acetonitrile by visible light irradiation (Table 1). As a model reaction, the oxidative coupling of benzylamine afforded N-benzylidenebenzylamine with a conversion of 99% after 16 h (Table 1, entry1), which revealed the great oxidation ability of **Cat-1** in such a heterogeneous system, considering the extremely simple workup. Table S4 summarizes the photocatalytic ability of reported materials in recent years in oxidative coupling of benzylamine. It indicates that **Cat-1** is notably more active than the reported catalysts based on other photosensitizers. Especially,

Table 1
Optimization of the conditions for photocatalytic oxidative homocoupling of Benzylamine.[a]

Entry	Catalyst	Yield (%)[b]	TON[c]	TOF/h^{-1}[d]
1	**Cat-1**	**99**	**3571**	**223**
2	**Cat-1**[e]	**–**	**–**	**–**
3	**blank**	**–**	**–**	**–**
4	**$K_5[BW_{12}O_{40}]$**	**8**	**160**	**10**
5	**DPNDI**	**16**	**36**	**2.3**
6	***L*–PYI**	**–**	**–**	**–**
7	**POM/DPNDI/PYI**	**22**	**–**	**–**
8	**Cat-1**[f]	**97**	**3499**	**218**
9	**Cat-1**[g]	**92**	**3318**	**207**
10	**Cat-1**[h]	**87**	**3138**	**196**

[a] Reaction conditions: Amine (5 mmol), **Cat-1** (10 mg, 14 μmol, 0.03 mol%), 10 W white LED lamp; room temperature, CH_3CN 3 mL, in air, 16 h.
[b] Yield determined by ^1H NMR spectroscopy of the crude products.
[c] Turnover number, calculated by the ratio of moles of product/mol of catalyst.
[d] Turnover frequency.
[e] No light.
[f] The yield of the second run.
[g] The yield of the third run.
[h] The yield of the fifth run.

compared with Zn–PDI (TON of 74, TOF of 18.5), **Cat-1** exhibiting great performance might owing to the incorporation of electron donor, *L*–PYI and electron acceptor, POM, which not only increases the probability of conPET, but also improves charge separation. [40]

The control experiments indicated that only traces of the target product were detected without light or **Cat-1** (Table 1, entries 2, 3). In addition, utilizing only $K_5[BW_{12}O_{40}]\cdot 5H_2O$, DPNDI or *L*–PYI provides 8%, 16% and trace yield, respectively (Table 1, entries 4–6). The simple physical mixture of POM, DPNDI and PYI converts 22% of the substrate into the target product (Table 1, entry 7). The **Cat-1** solids were easily isolated from the reaction suspension by simple filtration. The removal of **Cat-1** by filtration after 12 h of irradiation shut down the reaction directly, with the filtrate affording no additional conversion over another 24 h of irradiation. This observation suggested that **Cat-1** was a true heterogeneous catalyst in the catalytic system. After five runs of reuse, **Cat-1** exhibited a moderate loss of reactivity (from 99% to 87% yield (Table 1, entry 10), which indicated excellent recycling stability of **Cat-1**. The PXRD pattern of the **Cat-1** filtered from the reaction mixture matched well with the fresh one, which suggested the maintenance of the POMOF framework (Fig. S1).

When N_2 replaced air, benzylamine was hardly converted into the corresponding product, indicating the vital role of O_2 in the reaction process (Table 2, entry 1). The new characteristic UV–vis

Table 2
Photocatalytic oxidative coupling reaction of benzylamine by **Cat-1**[a].

Entry	1	2[c]	3[d]	4[e]	5[f]
Cat-1	+	+	+	+	+
hv	+	+	+	+	+
air	**N_2**	+	+	+	+
Yield(%)[b]	**–**	**10**	**21**	**8**	**42**

[a] Reaction conditions: Amine (5 mmol), **Cat-1** (10 mg, 14 μmol, 0.03 mol%), 10 W white LED lamp; room temperature, CH_3CN 3 mL, in air, 16 h.
[b] Yield determined by ^1H NMR spectroscopy of the crude products.
[c] **DABCO** as the single oxygen scavenger.
[d] Benzoquinone (**BQ**) as the superoxide scavenger.
[e] Isopropanol (**IPA**) as the ·OH scavenger.
[f] KI as the hole scavenger.

peaks of at 370 and 652 nm corresponding with oxidized tetramethylbenzidine (**TMB**) demonstrates the moderate oxidation power of **Cat-1** (Fig. S10) [41]. When $^1O_2$ scavenger, 1,4-diazabicyclo [2.2.2]octane (**DABCO**), was added to the reaction mixture, a 10% conversion was observed [42] (Table 2, entry 2) While in presence of $O_2^{\cdot-}$ scavenger *p*-Benzoquinone (**BQ**) [43], a 21% yield was observed (Table 2, entry 3). Compared with previous report [15], which the yield decreased slightly after adding BQ, $O_2^{\cdot-}$ showed great effect in this work. It might attribute to linker-to-cluster charge transfer (LCCT) process among POM and NDI, along with the generation of POM_{red}. [27,38] In addition, 2,2,6,6-Tetramethyl-1-piperidinyloxy (TEMPO) and 5,5-dimethyl-pyrroline-N-oxide (DMPO) were employed as the classical $^1O_2$ and $O_2^{\cdot-}$ probes, respectively, further manifesting the $^1O_2$ and $O_2^{\cdot-}$ formation over **Cat-1** (Fig. S11). Besides, the formed $^1O_2$ and $O_2^{\cdot-}$ would further generate H_2O_2 with the hydrogen abstract from substrates or solvent [44]. Using isopropanol (**IPA**) as a hydroxyl radical (·OH) scavenger, the product yield decreased significantly to 8% (Table 2, entry 4) [45]. Thus, we surmised ·OH that generated from H_2O_2 as a side product in the oxidative coupling reaction played a particular role in the reaction process. Therefore, all the obtained results corroborate each other and reveal that active $^1O_2$ and $O_2^{\cdot-}$ species are indeed formed in our reaction system and that the synergy of $^1O_2$ and $O_2^{\cdot-}$ in the oxidation of **Cat-1** is plausible. Besides, by adding KI as the hole scavenger, a low conversion of 42% was achieved (Table 2, entry 5) [46]. It's indicated that charge separation is also an important role in this work.

Spectroscopic investigations were further performed in order to understand the mechanism of the catalytic cycle. The UV/Vis spectra of **Cat-1** after irradiation exhibit some intense absorption bands centered at 509, 628 and 780 nm, which confirms the formation of the $DPNDI^{\cdot-}$ species (Fig. 2a) [47]. A shoulder at about 686 nm indicates the intermolecular charge-transfer (CT) between PYI and DPNDI [48]. The gradually reduced strength of the emission of **Cat-1** under visible light irradiation also verifies the electron transfer from PYI to DPNDI (Fig. 2b) [22]. The incorporation of PYI improves the charge transfer among the POMOF, thereby the generated radical anion $DPNDI^{\cdot-}$ is more stable than previous reported that only exist in N_2 atmosphere [8,9], thus increasing the probability of the next PET process. Besides, after adding benzylamine and light irradiated 30 min, the absorption bands increased obviously, which indicates PET process also happen among benzylamine and DPNDI. The blue-shift absorption bands at about 750 nm is assigned to W(V) d-d transitions and W(V)–W(VI) intervalence charge transfer (IVCT) transitions in the reduced anionic ligand [49–50], which is consistent with X-ray photoelectron spectroscopy (XPS).

XPS analysis revealed that the tungstate atoms experienced partial reduction under natural or UV–visible light in **Cat-1**. The main doublets of W 4f peak in fresh (37.45 and 35.3 eV, Fig. 2c) and irradiated ZnW–DPNDI–**PYI** (37.50 and 35.35 eV, Fig. 2d) were located between the reported values of W(VI) ions. Compared with fresh ZnW–DPNDI–**PYI**, the slight low-energy shifts of the XPS in irradiated ZnW–DPNDI–**PYI** relative to the reduction of tungsten are in accord with more W(V) ions. Note that, in irradiated ZnW–DPNDI–**PYI**, the W 4f peak displayed additional contributions at 36.82 and 34.67 eV, which can be contributed to more reduction of tungsten atoms after visible light irradiation. [51–52] Beyond that, the more negative potential of the intermediate $[BW^{VI}_{11}W^{V}O_{40}]^{6-}$ ($E[BW^{VI}_{12}O_{40}]^{5-}/[BW^{VI}_{11}W^{V}O_{40}]^{6-}$) = −0.36 vs. NHE)

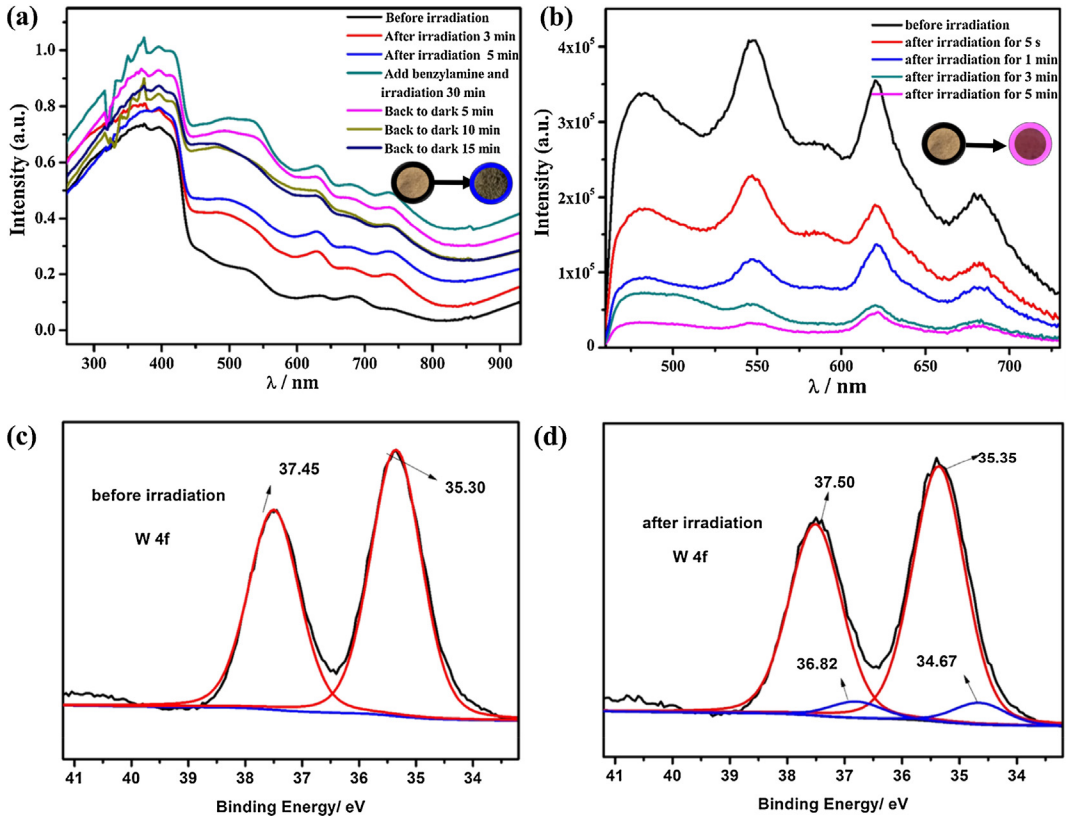

Fig. 2. (**a**) Formation of the DPNDI radical anion ($DPNDI^{\cdot-}$) and $[BW^{VI}_{11}W^{V}O_{40}]^{6-}$ upon photoexcitation (visible-light) of **Cat-1** in air. (**b**) Changes in the fluorescence spectra (in this case, intensity; Ex = 408 nm) of **Cat-1**, before and after irradiation. (**c and d**) Resolved W 4f XPS core-level spectra of **Cat-1** before and after irradiation with visible-light, respectively.

[53] than the reduction potential of O_2 to related reactive oxygen species (ROS, $E(O_2/O_2^{\cdot-})$ = –0.33 vs. NHE) [54], it is theoretically feasible for photocatalytic $O_2^{\cdot-}$ generation.

The Mott–Schottky measurements on **Cat-1** were performed at a frequency of 2000, 2500, and 3000 Hz, in order to further elucidate the semiconductor characters and the possibility for the photooxidation [55]. As shown in Fig. 3, the positive slope of the obtained C^{2-} values (vs the applied potentials) is consistent with those of typical n-type semiconductors [56]. The more negative potential of the LUMO level (–0.34 V vs. NHE) in **Cat-1** than the reduction potential for the conversion O_2 to $O_2^{\cdot-}$ further prove the possibility of forming $O_2^{\cdot-}$. Based on the Tauc plot (Fig. S12) [57], valence band (HOMO) was estimated to be 2.37 V vs NHE, which guarantees a high oxidation ability for benzylamine (E1/2(M^+/M) of +1.47 V vs. NHE) [58].

Upon the optimization of reaction conditions by using benzylamine as a probe substrate, to demonstrate the general applicability of **Cat-1**, different amines were examined (Table 3). When benzylamine was substituted with electron-donating substituents (—CH_3), a 99% conversion was achieved (Table 3, entry 2). However, the efficiency of benzylamine substituted with electron-withdrawing substituents (—F and —Cl) was decreased to 91% and 80% conversion, respectively (Table 3, entry 4). For heterocyclic amine that usually poison metal catalysts, it also can be well tolerated and displayed excellent yield (Table 3, entry 5). Secondary amine also gave an excellent yield (Table 3, entry 6). However, the oxidative coupling of aniline without a hydrogen atom at its α-carbon did not proceed (Table 3, entry 7), which suggested that reaction might occur via hydrogen abstraction.

Based on the unique features of the **Cat-1** and the above catalysis results, a possible cooperative catalytic mechanism is proposed (Scheme 2). Upon visible light photoexcitation DPNDI photooxidizes benzylamine, giving the radical anion $DPNDI^{\cdot-}$ and the benzylamine radical cation [14]. Continuous irradiation of the radical anion $DPNDI^{\cdot-}$ with visible light triggers a single electron transfer (SET) from the excited $DPNDI^{\cdot-*}$ to $[BW_{12}(VI)O_{40}]^{5-}$ producing the $[BW_{11}W(V)O_{40}]^{6-}$ and regenerating the neutral DPNDI [27]. Simultaneously, the photogenerated electrons of DPNDI can activate O_2 via an energy transfer yielding $^1O_2$ [29]. The holes in the valence band of DPNDI also oxidized the benzylamine to benzylamine radical cation and the electron in the conduction band of DPNDI reduced the $[BW_{12}(VI)O_{40}]^{5-}$ to $[BW_{11}W(V)O_{40}]^{6-}$. Along with the reoxidation of the $[BW_{11}W(V)O_{40}]^{6-}$ by O_2, $O_2^{\cdot-}$ was generated. The formed ROS ($^1O_2$ and $O_2^{\cdot-}$) would abstract the benzylic hydrogen from the benzylamine radical cation to produces the intermediate imine and H_2O_2 [44]. H_2O_2 further dissociated into ·OH, which play a supportive role in the oxidation of benzylamine

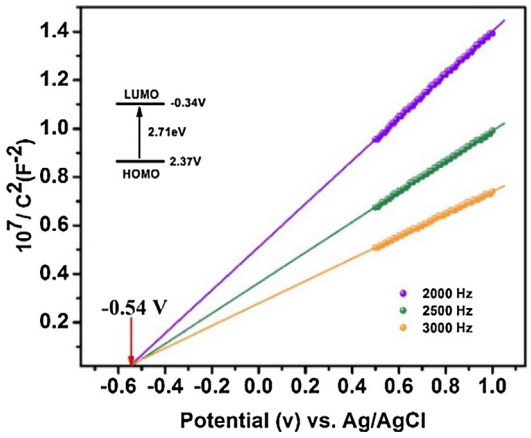

Fig. 3. Mott–Schottky plots for **Cat-1** in 0.1 M Na_2SO_4 aqueous solution.

Table 3
Photocatalytic oxidative coupling of various amines into imines.[a]

Entry	Substrate	Product	Yield(%)[b]	TOF/h^{-1}[c]
1		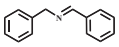	99	223
2	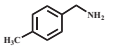	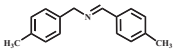	99	223
3		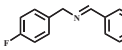	91	205
4		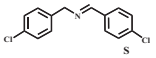	80	180
5		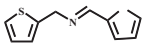	84	189
6	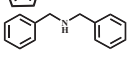	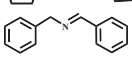	99	223
7		–	–	–

[a] Reaction conditions: Amine (5 mmol), **Cat-1** (10 mg, 14 μmol, 0.03 mol%), 10 W white LED lamp; room temperature, CH_3CN 3 mL, in air, 16 h.
[b] Yield determined by ^1H NMR spectroscopy of the crude products.
[c] Turnover frequency, calculated by the ratio of moles of product/mol of catalyst per hour.

to the corresponding imine. Then, the imine reacts with an additional amine molecule to produce the desired product after removal of ammonia.

Although the synergy of $^1O_2$ and $O_2^{\cdot-}$ have been reported in the photocatalytic oxidative homocoupling of amines into imines, the application in epoxidation is still in dark, due to the inferior selectivity of olefins oxidation with O_2 [59–61]. The catalytic performance of **Cat-1** in the epoxidation reaction of styrene with air as oxidant in CH_3CN, along with the heterogeneous reaction of **Cat-1** (0.03% mol ratio) at room temperature, was initially studied (Table 4). After 20 h of visible-light irradiation with a 10 W white LED lamp as light source, a 92% yield of epoxidation product was obtained and a 7% benzaldehyde, the result revealed the successful implementation of our POMOF design (Table 4, entry 1).

Control experiments and recycle tests clearly revealed the photocatalytic and heterogeneous nature (Table S5, entries 1–4). Using DPNDI or $K_5[BW_{12}O_{40}]\cdot 5H_2O$ as a homogenous catalyst with one organocatalytic reaction center could initiate the reaction and afford epoxide with a 20% and 12% yield under similar reaction conditions, respectively (Table S5, entries 5, 6). The use of DPNDI, *L*–PYI and $K_5[BW_{12}O_{40}]\cdot 5H_2O$ as multicomponent catalysts provided 34% yield of epoxide (Table S5, entry 7). Adding different ROS scavengers, the yields are decreased differently. Especially, the addition of IPA as ·OH scavenger, the selectivity decreased significantly (Table 4, entry 4). The control experiment utilizing H_2O_2 as oxidant in the styrene oxidation was carried out in the dark. The result showed a 99% yield of epoxide achieved after 24 h. The above results demonstrated H_2O_2 was help for the generation of the peroxide tungstate intermediates. Therefore, compared to UiO-66-NH_2 (Selectivity, 16.5%, Table S6, entry 2) [47], the high selectivity of this work was owing to the generation of H_2O_2, which will activate the corresponding W=O_t to generate an active peroxide tungstate intermediate. The IR spectra of **Cat-1** obtained in photocatalytic epoxidation process generated some new bands, which are corresponding with the O—O vibration bands. The results further proved the generation of peroxide tungstate intermediates, as reference reported [62]. Besides, the PYI moieties not only function as an electron donor to improve conPET, but also activate the W=O_t bond to improve the generation of the intermediate through the hydrogen bonds between the pyrrolidine N atom and the terminal oxygen atoms of $[BW_{12}O_{40}]^{5-}$ [63]. Thereby, the

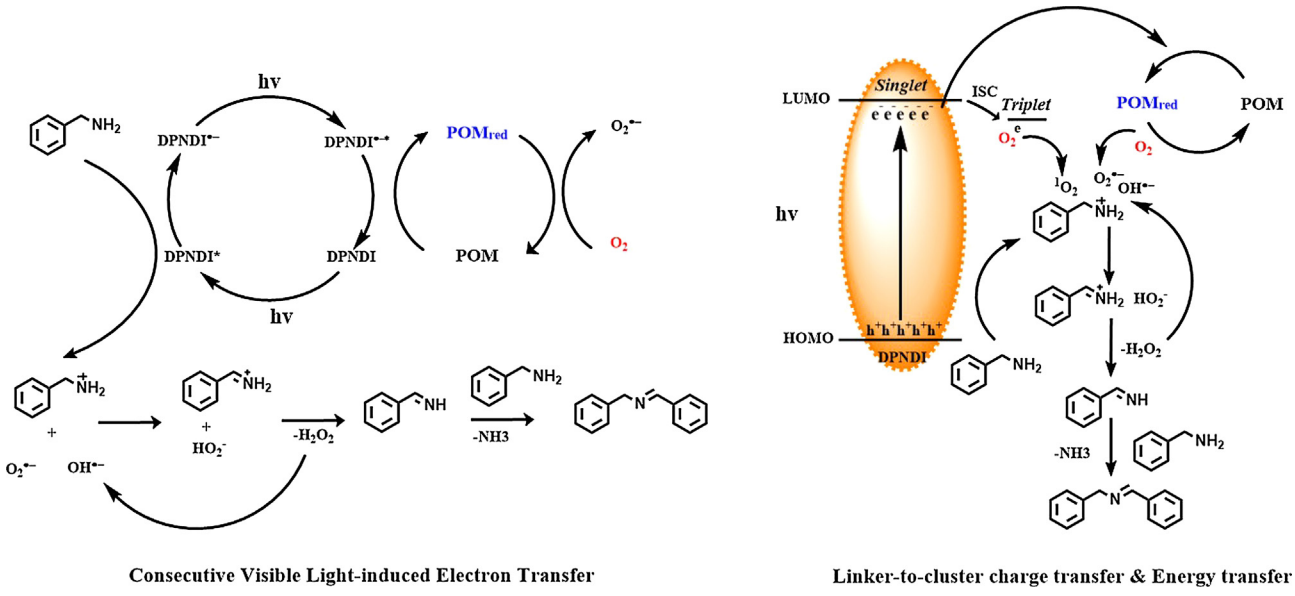

Scheme 2. Proposed catalytic mechanism.

Table 4
Conversion and selectivity in the photocatalysis oxidation of styrene with different oxidant, catalyst and radical scavenger.[a]

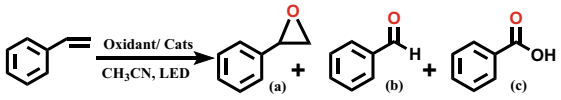

Entry	Control	Yield[b]			Sel.(%)[b]
		a	b	c	
1	Air	92	7	–	92
2	Air/DABCO[c]	30	4	–	88
3	Air/BQ[d]	34	5	–	86
4	Air/IPA[e]	20	5	57	25
5	Air/KI[f]	–	–	–	–

[a] Reaction conditions: Styrene (5 mmol), **Cat-1** (10 mg, 14 μmol, 0.03 mol%), 10 W white LED lamp; room temperature, CH_3CN 3 mL, in air, 20 h.
[b] Yield determined by ^1H NMR spectroscopy of the crude products.
[c] **DABCO** as the single oxygen scavenger.
[d] Benzoquinone (**BQ**) as the superoxide scavenger.
[e] Isopropanol as the ·OH scavenger.
[f] KI as the hole scavenger.

higher efficiency and selectivity of the reaction catalyzed by **Cat-1** may be attributed to the orderly distribution and spatial matching of the multi-catalytic groups, which simultaneously facilitate charge transfer among internal components and effectively bind and orient with substrates and O_2, respectively. The use of this catalyst can be extended to other substituted styrene substrates with comparable activity and selectivity (Table S7).

4. Conclusion

In summary, we have developed a powerful approach to construct ternary supramolecular system for prospective practical photocatalytic applications by assembling a functional photosensitizer, electron donor and electron acceptor into one single framework. The photocatalyst obtained with this strategy possesses the conPET process, good stability and long-lived charge-separated state. It exhibits high efficiency and selectivity in visible-light photocatalytic oxidation utilizing air under ambient conditions. This work opens up a new route for design and construction of excellent solid catalysts at the molecular level and expands the scope of MOFs as heterogeneous photocatalysts.

Acknowledgements

This work was supported by the National Natural Science Foundation of China (NSFC, Nos.21601048 and 21573056), the Natural Science Foundation of Henan Province (162300410012). We thank Dr. Shunjun Li, and Bo Qi for the spectra measurements.

Declaration of Competing Interest

The authors declare no conflict of interest.

Appendix A. Supplementary material

Supplementary data to this article can be found online at https://doi.org/10.1016/j.jcat.2019.06.040.

References

[1] Y.Z. Chen, Z.U. Wang, H. Wang, J. Lu, S.H. Yu, H.L. Jiang, Singlet oxygen-engaged selective photo-oxidation over Pt nanocrystals/porphyrinic MOF: the roles of photothermal effect and Pt electronic state, J. Am. Chem. Soc. 139 (2017) 2035–2044.
[2] M. Zhao, X.W. Zhang, C.D. Wu, Structural transformation of porous polyoxometalate frameworks and highly efficient biomimetic aerobic oxidation of aliphatic alcohols, ACS Catal. 7 (2017) 6573–6580.
[3] M.Q. Yang, Y.J. Xu, Selective photoredox using graphene-based composite photocatalysts, Phys. Chem. Chem. Phys. 15 (2013) 19102–19118.
[4] K. Czelej, K. Cwieka, J.C. Colmenares, K.J. Kurzydlowski, Y.J. Xu, Toward a comprehensive understanding of enhanced photocatalytic activity of the bimetallic PdAu/TiO_2 catalyst for selective oxidation of methanol to methyl formate, ACS Appl. Mater. Interfaces 9 (2017) 31825–31833.
[5] N. Huang, H. Drake, J. Li, J. Pang, Y. Wang, S. Yuan, Q. Wang, P. Cai, J. Qin, H.-C. Zhou, Flexible and hierarchical metal-organic framework composites for high-performance catalysis, Angew. Chem. Int. Ed. 57 (2018) 8916–8920.
[6] Y. Zhang, N. Zhang, Z.R. Tang, Y.J. Xu, Transforming CdS into an efficient visible light photocatalyst for selective oxidation of saturated primary C-H bonds under ambient conditions, Chem. Sci. 3 (2012) 2812–2822.
[7] P. Bai, X. Tong, J. Wan, Y. Gao, S. Xue, Flower-like $Bi_2O_2CO_3$-mediated selective oxidative coupling processes of amines under visible light irradiation, J. Catal. 374 (2019) 257–265.

[8] Y. Zhi, K. Li, H. Xia, M. Xue, Y. Mu, X. Liu, Robust porous organic polymers as efficient heterogeneous organo-photocatalysts for aerobic oxidation reactions, J. Mater. Chem. A. 5 (2017) 8697–8704.

[9] C. Xu, H. Liu, D. Li, J.H. Su, H.L. Jiang, Direct evidence of charge separation in a metal–organic framework: efficient and selective photocatalytic oxidative coupling of amines *via* charge and energy transfer, Chem. Sci. 9 (2018) 3152–3158.

[10] V.R. Battula, H. Singh, S. Kumar, I. Bala, S.K. Pal, K. Kailasam, Natural sunlight driven oxidative homocoupling of amines by a truxene-based conjugated microporous polymer, ACS Catal. 8 (2018) 6751–6759.

[11] A. Thakur, R. Baba, T. Wada, P. Chammingkwan, T. Taniike, Cooperative catalysis by multiple active centers of a half-titanocene catalyst integrated in polymer random coils, ACS Catal. 9 (2019) 3648–3656.

[12] Y.X. Tan, Y.P. He, D. Yuan, J. Zhang, Use of aligned triphenylamine-based radicals in a porous framework for promoting photocatalysis, Appl. Catal. B: Environ. 221 (2018) 664–669.

[13] I. Ghosh, B. König, Chromoselective photocatalysis: controlled bond activation through light-color regulation of redox potentials, Angew. Chem. Int. Ed. 55 (2016) 7676–7679.

[14] I. Ghosh, T. Ghosh, J.I. Bardagi, B. Konig, Reduction of aryl halides by consecutive visible light-induced electron transfer processes, Science. 346 (2014) 725–728.

[15] L. Zeng, T. Liu, C. He, D. Shi, F. Zhang, C. Duan, Organized aggregation makes insoluble perylene diimide efficient for the reduction of aryl halides via consecutive visible light-induced electron-transfer processes, J. Am. Chem. Soc. 138 (2016) 3958–3961.

[16] H. Li, Y. Yang, C. He, L. Zeng, C. Duan, Mixed-Ligand metal-organic framework for two-photon responsive photocatalytic C-N and C–C coupling reactions, ACS Catal. 9 (2019) 422–430.

[17] J.-L. Wang, C. Wang, W. Lin, Metal-organic frameworks for light harvesting and photocatalysis, ACS Catal. 2 (2012) 2630–2640.

[18] T. Zhang, Y. Jin, Y. Shi, M. Li, J. Li, C. Duan, Modulating photoelectronic performance of metal–organic frameworks for premium photocatalysis, Coord. Chem. Rev. 380 (2019) 201–229.

[19] Y. Liu, Z. Liu, D. Huang, M. Cheng, G. Zeng, C. Lai, C. Zhang, C. Zhou, W. Wang, D. Jiang, H. Wang, B. Shao, Metal or metal-containing nanoparticle@MOF nanocomposites as a promising type of photocatalyst, Coord. Chem. Rev. 388 (2019) 63–78.

[20] M.A. Kobaisi, S.V. Bhosale, K. Latham, A.M. Raynor, S.V. Bhosale, Functional naphthalene diimides: synthesis, properties, and applications, Chem. Rev. 116 (2016) 11685–11796.

[21] D. Gosztola, M.P. Niemczyk, W. Svec, A.S. Lukas, M.R. Wasielewski, Excited doublet states of electrochemically generated aromatic imide and diimide radical anions, J. Phys. Chem. A. 104 (2000) 6545–6551.

[22] S.S. Wang, G.Y. Yang, Recent advances in polyoxometalate-catalyzed reactions, Chem. Rev. 115 (2015) 4893–4962.

[23] D. Ravelli, S. Protti, M. Fagnoni, Decatungstate anion for photocatalyzed "window ledge" reactions, Acc. Chem. Res. 49 (2016) 2232–2242.

[24] Y.V. Geletii, C.L. Hill, R.H. Atalla, I.A. Weinstock, Reduction of O_2 to superoxide anion ($O_2^{\bullet-}$) in water by heteropolytungstate cluster-anions, J. Am. Chem. Soc. 128 (2006) 17033–17042.

[25] J.A. Terrett, M.D. Clift, D.W.C. MacMillan, Direct β-alkylation of aldehydes via photoredox organocatalysis, J. Am. Chem. Soc. 136 (2014) 6858–6861.

[26] F.R. Petronijević, M. Nappi, D.W.C. MacMillan, Direct β-functionalization of cyclic ketones with aryl ketones via the merger of photoredox and organocatalysis, J. Am. Chem. Soc. 135 (2013) 18323–18326.

[27] J.Z. Liao, C. Wu, X.Y. Wu, S.Q. Deng, C.Z. Lu, Exceptional photosensitivity of a polyoxometalate-based charge-transfer hybrid material, Chem. Commun. 52 (2016) 7394–7397.

[28] A. Pal, I. Ghosh, S. Sapra, B. König, Quantum dots in visible-light photoredox catalysis: reductive dehalogenations and C-H arylation reactions using aryl bromides, Chem. Mater. 29 (2017) 5225–5231.

[29] F. Doria, I. Manet, V. Grande, S. Monti, M. Freccero, Water-soluble naphthalene diimides as singlet oxygen sensitizers, J. Org. Chem. 78 (2013) 8065–8073.

[30] S. Luo, Mi, X.L. Zhang, S. Liu, H. Xu, J.P. Cheng, Functionalized chiral ionic liquids as highly efficient asymmetric organocatalysts for Michael addition to nitroolefins, Angew. Chem. Int. Ed. 45 (2006) 3093–3097.

[31] G.B. Li, J.M. Liu, Z.Q. Yu, W. Wang, C.Y. Su, Assembly of a 1D coordination polymer through in situ formation of a new ligand by double C−C coupling on $CHCl_3$ under solvothermal conditions, Inorg. Chem. 48 (2009) 8659–8661.

[32] C.R. Deltcheff, M. Fournier, R. Franck, R. Thouvenot, Vibrational investigations of polyoxometalates. 2. Evidence for anion-anion interactions in molybdenum (VI) and tungsten(VI) compounds related to the Keggin structure, Inorg. Chem. 22 (1983) 207–216.

[33] G.M. Sheldrick, SHELXTL97, Program for Crystal Structure Solution, University of Göttingen, Göttingen, Germany, 1997.

[34] SMART, Data collection software (version 5.629), Bruker AXS Inc., Madison, WI, 2003.

[35] SAINT, Data reduction software (version 6.45), Bruker AXS Inc., Madison, WI, 2003.

[36] Q. Han, B. Qi, W. Ren, C. He, J. Niu, C. Duan, Polyoxometalate-based homochiral metal-organic frameworks for tandem asymmetric transformation of cyclic carbonates from olefins, Nat. Commun. 6 (2015) 10007.

[37] A.L. Spek, Single-crystal structure validation with the program PLATON, J. Appl. Cryst. 36 (2003) 7–13.

[38] H.L. Zhang, J.Z. Liao, W. Yang, X.Y. Wu, C.Z. Lu, A novel naphthalenediimide-based lanthanide–organic framework with polyoxometalate templates exhibiting reversible photochromism, Dalton Trans. 46 (2017) 4898–4901.

[39] J.Z. Liao, H.L. Zhang, S.S. Wang, J.P. Yong, X.Y. Wu, R. Yu, C.Z. Lu, Multifunctional radical-doped polyoxometalate-based host-guest material: photochromism and photocatalytic activity, Inorg. Chem. 54 (2015) 4345–4350.

[40] B. Matt, J. Fize, J. Moussa, H. Amouri, A. Pereira, V. Artero, G. Izzet, A. Proust, Charge photo-accumulation and photocatalytic hydrogen evolution under visible light at an iridium(iii)-photosensitized polyoxotungstate, Energy Environ. Sci. 6 (2013) 1504–1508.

[41] P.D. Josephygg, T. Elingg, R.P. Mason, The horseradish peroxidase-catalyzed oxidation of 3,5,3′5′-tetramethylbenzidine, J. Biol. Chem. 257 (1982) 3669–4675.

[42] Y. Yamakoshi, N. Umezawa, A. Ryu, K. Arakane, N. Miyata, Y. Goda, T. Masumizu, T. Nagano, Active OXYGEN species generated from photoexcited fullerene (C60) as potential medicines: $O_2^{\cdot-}$ versus $^1O_2$, J. Am. Chem. Soc. 125 (2003) 12803–12809.

[43] C. Qi, X. Liu, J. Ma, C. Lin, X. Li, H. Zhang, Activation of peroxymonosulfate by base: Implications for the degradation of organic pollutants, Chemosphere 151 (2016) 280–288.

[44] O. Jung, M.L. Pegis, Z. Wang, G. Banerjee, C.T. Nemes, W.L. Hoffeditz, J.T. Hupp, C.A. Schmuttenmaer, G.W. Brudvig, J.M. Mayer, Highly active NiO photocathodes for H_2O_2 production enabled via outer-sphere electron transfer, J. Am. Chem. Soc. 140 (2018) 4079–4084.

[45] H.-F. Shi, G. Yan, Y. Zhang, H.Q. Tan, W.Z. Zhou, Y.Y. Ma, Y.-G. Li, W. Chen, E.-B. Wang, $Ag/Ag_xH_{3-x}PMO_{12}O_{40}$ nanowires with enhanced visible-light-driven photocatalytic performance, ACS Appl. Mater. Interfaces. 9 (2017) 422–430.

[46] O. Zandi, T.W. Hamann, Determination of photoelectrochemical water oxidation intermediates on haematite electrode surfaces using operando infrared spectroscopy, Nat. Chem. 8 (2016) 778–783.

[47] Y. Takashima, S. Furukawa, S. Kitagawa, Control of the charge-transfer interaction between a flexible porous coordination host and aromatic guests by framework isomerism, CrystEngComm 13 (2011) 3360–3363.

[48] B.A. Johnson, A. Bhunia, H. Fei, S.M. Cohen, S. Ott, Development of a UiO-type thin film electrocatalysis platform with redox-active linkers, J. Am. Chem. Soc. 140 (2018) 2985–2994.

[49] C. Zhao, Z. Huang, W. Rodríguez-Córdoba, C.S. Kambara, K.P. O'Halloran, K.I. Hardcastle, D.G. Musaev, T. Lian, C.L. Hill, Synthesis and characterization of a metal-to-polyoxometalate charge transfer molecular chromophore, J. Am. Chem. Soc. 133 (2011) 20134–20137.

[50] W. Sun, B. An, B. Qi, T. Liu, M. Jin, C. Duan, Dual-excitation polyoxometalate-based frameworks for one-pot light-driven hydrogen evolution and oxidative dehydrogenation, ACS Appl. Mater. Interfaces 10 (2018) 13462–13469.

[51] Y. Nagaoka, S. Shiratori, Y. Einaga, Photo-control of adhesion properties by detachment of the outermost layer in layer-by-layer assembled multilayer films of preyssler-type polyoxometalate and polyethyleneimine, Chem. Mater. 20 (2008) 4004–4010.

[52] D. Mercier, S. Boujday, C. Annabi, R. Villanneau, C.-M. Pradier, A. Proust, Bifunctional polyoxometalates for planar gold surface nanostructuration and protein immobilization, J. Phy. Chem. C. 116 (2012) 13217–13224.

[53] D.C. Duncan, M. Anne Fox, Early Events in decatungstate photocatalyzed oxidations: a nanosecond laser transient absorbance reinvestigation, J. Phys. Chem. A. 102 (1998) 4559–4567.

[54] W. Huang, B.C. Ma, H. Lu, R. Li, L. Wang, K. Landfester, K.A.I. Zhang, Visible-light-promoted selective oxidation of alcohols using a covalent triazine framework, ACS Catal. 7 (2017) 5438–5442.

[55] Y.X. Pan, Y. You, S. Xin, Y.T. Li, G.T. Fu, Z.M. Cui, Y.L. Men, F.F. Cao, S.H. Yu, J.B. Goodenough, Photocatalytic CO_2 reduction by carbon-coated indium-oxide nanobelts, J. Am. Chem. Soc. 139 (2017) 4123–4129.

[56] C. Han, Z.R. Tang, J. Liu, S. Jin, Y.J. Xu, Efficient photoredox conversion of alcohol to aldehyde and H_2 by heterointerface engineering of bimetal–semiconductor hybrids, Chem. Sci. 10 (2019) 3514–3522.

[57] X.K. Wang, J. Liu, L. Zhang, L.Z. Dong, S.L. Li, Y.H. Kan, D.-S. Li, Y.Q. Lan, Monometallic catalytic models hosted in stable metal-organic frameworks for tunable CO_2 photoreduction, ACS Catal. 9 (2019) 1726–1732.

[58] J.A. Johnson, J. Luo, X. Zhang, Y.-S. Chen, M.D. Morton, E. Echeverría, F.E. Torres, J. Zhang, Porphyrin-metalation-mediated tuning of photoredox catalytic properties in metal-organic frameworks, ACS Catal. 5 (2015) 5283–5291.

[59] J. Long, S. Wang, Z. Ding, S. Wang, Y. Zhou, L. Huang, X. Wang, Amine-functionalized zirconium metal–organic framework as efficient visible-light photocatalyst for aerobic organic transformations, Chem. Commun. 48 (2012) 11656–11658.

[60] Y. Zhang, N. Zhang, Z.-R. Tang, Y.J. Xu, Graphene transforms wide band gap ZnS to a visible light photocatalyst. The new role of graphene as a macromolecular photosensitizer, ACS Nano 6 (2012) 9777–9789.

[61] D. Malko, Y. Guo, P. Jones, G. Britovsek, A. Kucernak, Heterogeneous iron containing carbon catalyst (Fe-N/C) for epoxidation with molecular oxygen, J. Catal. 370 (2019) 357–363.

[62] J. Guo, Y. Niu, L. Song, Q. Xu, J. Lu, P. Ma, D. Zhang, C. Zhang, J. Niu, J. Wang, Synthesis, characterization and catalytic epoxidation properties of lanthanide-stabilized peroxoisopolytungstates, Dalton Trans. 46 (2017) 12981–12987.

[63] Q. Han, C. He, M. Zhao, B. Qi, J. Niu, C. Duan, Engineering chiral polyoxometalate hybrid metal-organic frameworks for asymmetric dihydroxylation of olefins, J. Am. Chem. Soc. 135 (2013) 10186–10189.